

# Reconstruction of the Dark Energy equation of state from latest data: the impact of theoretical priors.

Francesca Gerardi,<sup>a,b,1</sup> Matteo Martinelli,<sup>b</sup> Alessandra Silvestri<sup>b</sup>

<sup>a</sup>Dipartimento di Fisica ed Astronomia “Galileo Galilei”, Università di Padova,  
Vicolo Osservatorio 3, I-35122 Padova, Italy

<sup>b</sup>Institute Lorentz, Leiden University, PO Box 9506, Leiden 2300 RA, The Netherlands

E-mail: [francesca.gerardi@studenti.unipd.it](mailto:francesca.gerardi@studenti.unipd.it), [martinelli@lorentz.leidenuniv.nl](mailto:martinelli@lorentz.leidenuniv.nl),  
[silvestri@lorentz.leidenuniv.nl](mailto:silvestri@lorentz.leidenuniv.nl)

**Abstract.** We reconstruct the Equation of State of Dark Energy (EoS) from current data using a non-parametric approach where, rather than assuming a specific time evolution of this function, we bin it in time. We treat the transition between the bins with two different methods, i.e. a smoothed step function and a Gaussian Process reconstruction, investigating whether or not the two approaches lead to compatible results. Additionally, we include in the reconstruction procedure a correlation between the values of the EoS at different times in the form of a theoretical prior that takes into account a set of viability and stability requirements that one can impose on models alternative to  $\Lambda$ CDM. In such case, we necessarily specialize to broad, but specific classes of alternative models, i.e. Quintessence and Horndeski gravity. We use data coming from CMB, Supernovae and BAO surveys. We find an overall agreement between the different reconstruction methods used; with both approaches, we find a time dependence of the mean of the reconstruction, with different trends depending on the class of model studied. The constant EoS predicted by the  $\Lambda$ CDM model falls anyway within the  $1\sigma$  bounds of our analysis.

---

<sup>1</sup>Corresponding author.

---

## Contents

<b>1</b>	<b>Introduction</b>	<b>1</b>
<b>2</b>	<b>Non parametric reconstruction</b>	<b>2</b>
2.1	Smoothed step function	3
2.2	Gaussian Process	3
<b>3</b>	<b>Data and analysis method</b>	<b>5</b>
3.1	Theoretical correlation prior	6
<b>4</b>	<b>Results</b>	<b>8</b>
4.1	Quintessence	8
4.2	Horndeski class of MG models	10
<b>5</b>	<b>Conclusions</b>	<b>13</b>

---

## 1 Introduction

Since the discovery of the late time cosmic acceleration [1, 2], the physical mechanism underlying this accelerated phase has been an elusive one and still poses an open question for Cosmology. The simplest candidate that could drive this acceleration is a Cosmological Constant  $\Lambda$ , as in the  $\Lambda$ CDM model. Despite its success in describing cosmological observations [3], the  $\Lambda$ CDM model poses theoretical questions that still prompt the investigation of the nature of  $\Lambda$ , i.e. the value of this constant and the special moment of the Universe lifetime in which this starts to dominate over the other components [4, 5].

Furthermore, recent observations have reached a precision which started to highlight tensions between the measurements of  $\Lambda$ CDM parameters as inferred from different probes. The most striking one, appears in the values for the Hubble constant  $H_0$  found with local measurements [6] and with Cosmic Microwave Background (CMB) observations [3]. While the former directly measure the current rate of expansion, the latter rely on the assumption of a specific cosmological model ( $\Lambda$ CDM) to extrapolate high redshift measurements to present time. A similar tension, although less statistically significant, is also found when measuring the growth of cosmological perturbations from a high or low redshift point of view, relying again on CMB [3] versus galaxy surveys [7–9]. Even though it is not excluded that these tensions could be driven by systematic errors, it could also be that they are due to the assumption of the  $\Lambda$ CDM model in the analysis of high redshift data.

Many alternatives to the  $\Lambda$ CDM have been put to test against observations (see e.g. [10–15]) sometimes allowing to rule out specific theories [16–19], but more often leading only to constraints of their parameter space around the  $\Lambda$ CDM limit. Given the significant amount of available models and the difficulty in testing all of them against the data, a model independent approach is desirable. A typical example is the so-called Chevallier-Polarski-Linder (CPL) parameterization [20, 21], a simple two parameters description of the time-dependence of the equation of state for the component that dominates at late times and sources cosmic acceleration. We will generically refer to this component as Dark Energy (DE), and refer to its equation of state as  $w_{\text{DE}}$  (EoS). This could be an actual additional fluid contributing to

the energy-momentum tensor, or, alternatively, result from modifications of gravity (MG). In either cases, generally  $w_{\text{DE}}$  is expected to be non-zero. The CPL parameterization has been used extensively in the literature to constrain the time evolution of DE (see e.g. [3, 22–24]), and also to quantify the ability of future experiments to shed light on the nature of DE [25]. Even though this approach allows to investigate the DE problem without restricting to a specific theory, it still relies on assumptions on the time evolution of  $w_{\text{DE}}$ . An alternative approach is to reconstruct  $w_{\text{DE}}$  constraining its value at different times. This so-called “non-parametric” approach has been often used in literature [26–31] but the amount of free parameters needed to reconstruct the EoS has often hindered its usefulness.

In this paper, we take one step further and combine theoretical priors into the non-parametric reconstruction of  $w_{\text{DE}}$ , based on general requirements of physical viability [32]. These are derived for broad, but specific classes of theories. Hence, even though they are mild, including them in the reconstruction slightly limits the model independence. More importantly, the priors allow to introduce a, theoretically informed correlation between the values of  $w_{\text{DE}}$  at different times, aiding the reconstruction. Such an approach also guarantees that the reconstructed function will eventually correspond to a theoretically viable model, while it can be complicated to map a completely model independent reconstruction of the EoS to the one produced by any well behaved theory [33].

The paper is organized as follows. In Section 2 we outline the reconstruction techniques we exploited to obtain a model independent  $w_{\text{DE}}$  from binned values constrained through observational data. In Section 3 we describe the general data analysis methodology employed, we describe the theoretical information coming from viability requirements for two classes of alternatives to  $\Lambda$ CDM (Quintessence and Horndeski), and we detail how this information is included in our analysis. We then present the results of this reconstruction in Section 4, before drawing our conclusions in Section 5.

## 2 Non parametric reconstruction

We start discretizing the Dark Energy EoS,  $w_{\text{DE}}$ , into several binned values, with the value of  $w_{\text{DE}}$  in each bin being a free parameter of our analysis. The evolution of  $w_{\text{DE}}$  in time can be equivalently expressed in terms of the redshift  $z$  or of the scale factor  $a$ , which are connected to time through the Friedmann equations. In this paper we choose to discretize  $w_{\text{DE}}$  into bins equally spaced in the scale factor  $a$  (with  $w_{\text{DE}}(a_i) = w_i$  at the center of the  $i$ -th bin), in the interval  $[a_{\text{min}}, 1]$ . The choice of binning the EoS in scale factor rather than in redshift, as well as the specific choice of the binning strategy, is due to the analysis method that we will detail further in this paper, in particular to the use of theoretical viability priors (see Section 3.1). Indeed, accounting for theoretical considerations on the general behavior of  $w_{\text{DE}}(a)$  would set conditions on the reconstruction and on the correlation between the binned values of the function, e.g. motivating a correlation length  $\xi$  between the  $w_i$  and, consequently, the setting of the binning strategy [34]. We will describe the binning strategy more explicitly case by case in Section 3.1.

Cosmological observables generally do not depend directly on the values of  $w_{\text{DE}}$  at each redshift, but rather on the evolution in time of this function between the observer and the measured source. Therefore, we need to join the binned values into a function of time that can be, e.g., integrated. Let us use the luminosity distance  $d_L(a)$  inferred from observations

of standard candles to illustrate this point. It can be expressed as

$$d_L(a) = \frac{c}{aH_0} \int_a^1 \frac{da'}{E(a')} \quad (2.1)$$

with

$$E(a) \approx \sqrt{\Omega_m a^{-3} + \Omega_{\text{DE}} \exp \left[ \int_a^1 \frac{3[1 + w_{\text{DE}}(a')]}{a'} da' \right]}. \quad (2.2)$$

Clearly, if we are to fit a binned EoS to SNe data, we need to ensure a well defined evolution for  $w_{\text{DE}}$  by specifying how the function will behave within a certain bin and in moving from one to the other, in order to. In our analysis we interpolate the binned  $w_i$  values via two alternative techniques: a smoothed step function and Gaussian Process (GP), described in detail below. Indeed, once the binning properties for a specific case are given, we develop two different reconstructions, corresponding to the two different methods, and compare the results obtained.

## 2.1 Smoothed step function

The simplest choice to interpolate the binned values of  $w_{\text{DE}}$  is to use a step function. Defining  $w_{\text{DE}}(a_i) = w_i$  as the values of the EoS at the center of each bin,

$$w_{\text{DE}}(a) = \sum_{i=1}^{N-1} (w_{i+1} + w_i) [\theta_H(a - a_i) - \theta_H(a - a_{i+1})], \quad (2.3)$$

where  $\theta_H$  is the Heaviside function and  $N$  is the number of bins. With this choice the EoS is constant within each bin and it has a sharp transition in its value when moving from one bin to the next (see blue line in Figure 1).

Such a reconstruction can in principle cause numerical issues due to the fact that the function and its derivative are not well defined at the boundaries between bins. For this reason, we adopt a smoothed step function (see e.g. [35])

$$w_{\text{DE}}(a) = w_1 + \sum_{i=1}^{N-1} \frac{w_{i+1} - w_i}{2} \left\{ 1 + \tanh \left[ s \left( \frac{a - a_{i+1}}{a_{i+1} - a_i} \right) \right] \right\} \quad (2.4)$$

where  $N$  is the number of bins,  $s$  is a smoothing factor used to control the slope of the transition from one bin to the adjacent ones. In this work we set  $s = 10$ ; the resulting reconstruction can be seen in Figure 1 (green line).

## 2.2 Gaussian Process

In the smoothed step approach discussed above, the reconstructed function is assumed to be constant within each redshift bin; this can in principle bias the results obtained if the choice of the bin intervals is not done properly. To overcome such problem, one can rely on more sophisticated techniques, e.g. Gaussian Process. A GP is defined as a collection of random variables, any finite number of which have a joint Gaussian distribution [36]. Considering the training points  $\vec{a} = (a_1 \ a_2 \ a_3)$ , we can always think of the function  $w_{\text{DE}}(a)$  evaluated at these points as a vector and, at each point  $a_i$ ,  $w_i$  is a Gaussian random variable with mean

$\mu(a_i)$  and variance  $\sigma_{a,i}^2$ . The entire vector will then be modeled with a multivariate Gaussian distribution

$$\vec{w}_{\text{DE}} = \begin{bmatrix} w_1 \\ w_2 \\ w_3 \end{bmatrix} \sim \mathcal{N}(\vec{\mu}, C) = \mathcal{N}\left(\vec{\mu}, \begin{bmatrix} C_{11} & C_{12} & C_{13} \\ C_{21} & C_{22} & C_{23} \\ C_{31} & C_{33} & C_{33} \end{bmatrix}\right) \quad (2.5)$$

where  $\mathcal{N}$  stands for Normal distribution and  $C$  is the covariance matrix, with  $C_{ij} = C(w_i, w_j)$  denoting the correlation between two points  $a_i$  and  $a_j$ . We expect that the closer  $a_i$  and  $a_j$  are, the more the corresponding values of the EoS,  $w_i$  and  $w_j$ , will be correlated. In order to interpolate the training points we use the python package `sklearn`, which provides several choices for the covariance  $C$ , and we work here with the Radial Basis Function (RBF) :

$$C(a, a') = e^{-\frac{|a-a'|^2}{2\xi^2}} \quad (2.6)$$

where  $\xi$  is the correlation length, such that

$$C(a, a') = \begin{cases} 0 & |a - a'| \gg \xi \\ 1 & a = a' \end{cases} \quad (2.7)$$

Such a choice provides a Kernel for the GP which is both stationary, because it is a function of  $a - a'$ , and isotropic, since it is a function of its module  $|a - a'|$ . The reason why we chose this Kernel is that it is fully characterized by only one parameter, the correlation length  $\xi$ . Of course this results in a lower flexibility of our reconstruction, but it does not introduce new degeneracies associated to a high number of hyperparameters. Moreover, this kernel is infinitely differentiable, leading to the process being infinitely mean-square differentiable [36]. In this paper, we do not explore the dependence of our results on the choice of the GP Kernel, but rather leave this investigation for our ongoing work which extends to the reconstruction of the functions relevant for large scale structure.

Given a set of training points  $(a_i, w_i)$ , we want to obtain the value of the function at a point  $a_*$ , defined as  $w_*$ . Since we expect the function to be smooth, for a small variation of the  $a$  variable we do not expect the function at that point to differ much from its values in the adjacent points.

Assuming that  $w_*$  will be Gaussian distributed as well, i.e.  $w_* \sim \mathcal{N}(\mu_*, C(a_*, a_*))$ , where  $C(a_*, a_*)$  is the self-covariance, the joint distribution will assume the form of

$$\begin{bmatrix} \vec{w}_{\text{DE}} \\ w_* \end{bmatrix} \sim \mathcal{N}\left(\begin{bmatrix} \vec{\mu} \\ \mu_* \end{bmatrix}, \begin{bmatrix} C(\vec{a}, \vec{a}') & C(\vec{a}, a_*) \\ C(a_*, \vec{a}) & C(a_*, a_*) \end{bmatrix}\right) \quad (2.8)$$

After specifying the mean and correlation functions, considering now all the fitting points, the GP is defined as

$$w_{\text{DE}}(\vec{a}) \sim GP(\mu(\vec{a}), C(\vec{a}, \vec{a}')) \quad (2.9)$$

This reconstruction method does not require only the binned points  $a_i$  and  $w_i(a)$  as an input, but also specific choices for the mean and the correlation length of the Gaussian distribution. Usually, GPs are used on observational data where the training points are fixed (provided by the data), and therefore one can obtain  $\mu$  and  $\xi$  as the values providing the best fit of the reconstructed function to the observations (see e.g. [28, 37]). Here instead, while the  $a_i$  are fixed, the  $w_i$  values are free parameters of our analysis. Therefore we need to obtain different GP reconstructions for each sampled set of parameters  $w_i$ . In order to achieve this,

we choose to set the values of  $\mu$  and  $\xi$  to fixed a priori values, where the mean function is set to be  $\mu = w_\Lambda = -1$ , since the reconstructed function is expected to vary in the vicinity of -1. However, as long as multiple training points will be located within one correlation length  $\xi$ , the mean value is not going to significantly impact the behavior of the function and  $w_{DE}$  will tend to the mean, only where no training points are available, since the correlation drops off (see Eq. (2.7)). In Section 3.1 we will describe how limiting the analysis to general classes of models allows to obtain theoretically derived estimation of  $\xi$ , due to the demand that the reconstructed  $w_{DE}(a)$  can be eventually linked to a physically viable theoretical model. Even if they refer to kernels (Table 1) which are different from that of Eq. (2.6), we can assume that the extrapolated correlation length will be a good approximation for the GP reconstruction.

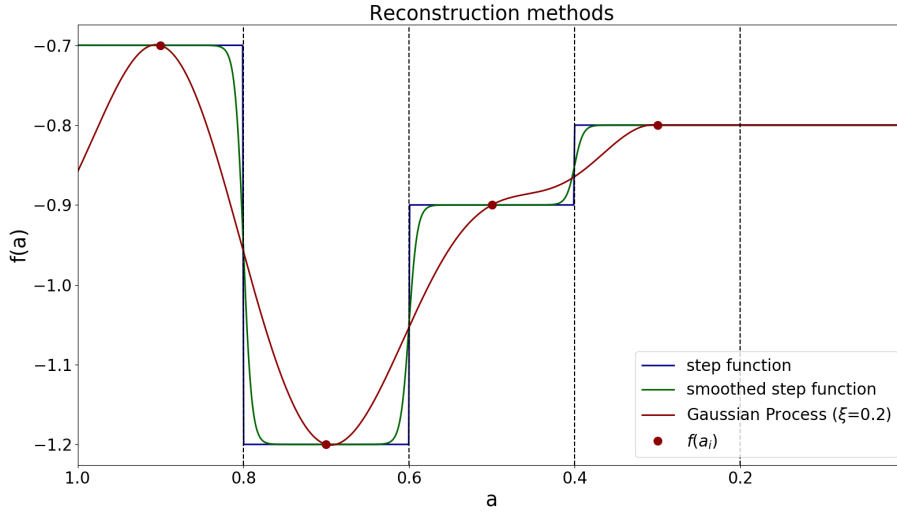


**Figure 1.** Reconstructed  $w_{DE}$  as a function of the scale factor, with three different methods: step function, smoothed step function and Gaussian Process; the red dots are the chosen  $w(a_i)$ . The values of  $w_{DE}$  at  $a < a_{min}$  are fixed to  $w_{DE}(a_{min})$ .

### 3 Data and analysis method

Given the binned  $w_{DE}$ , a reconstruction method and the standard set of cosmological parameters, we can make predictions for the desired cosmological observables and constrain our parameter space against data. To this extent, we use the public code **CAMB** [38, 39], modifying it in such a way that we can provide as an input the binned values of  $w_{DE}$  and the chosen reconstruction method. We then sample the entire parameter space with the public Monte Carlo Markov Chain (MCMC) code **CosmoMC** [40]. For the cosmological parameters, we choose those of the minimal flat  $\Lambda$ CDM cosmology: the baryon and cold dark matter densities at present day,  $\Omega_b h^2$  and  $\Omega_c h^2$ ; the optical depth,  $\tau$ ; the primordial power spectrum amplitude and tilt,  $A_s$  and  $n_s$ , and the Hubble parameter  $H_0$ . Alongside the standard cosmological parameters we also sample the binned values of the EoS  $w_i$ . The prior range and bins positions in scale factors will depend on the specific cases investigated and will be specified in

the following section; in general however, we assume that the EoS stays constant outside the binned interval, i.e.  $w(a > a_1) = w_1$  and  $w(a < a_N) = w_N$ . We use flat priors on all the parameters.

We use the following datasets: the JLA ('Joint Light-curve Analysis') dataset [41], that unifies Type Ia SNe observations of SDSS-II (Sloan Digital Sky Survey) [42] and SNLS (Supernova Legacy Survey) [43] collaborations, for a total of 740 Type Ia SNe up to redshift  $z \sim 1$ ; the 6dFGS (6dF Galaxy Survey) [44] and SDSS Data Release 7 [45] for BAO and Planck 2015 data [46] for CMB. We will specify in the following subsection the prior ranges for  $w_i$ , as well as the different combinations of the data listed above, depending on the different classes of theories under consideration.

### 3.1 Theoretical correlation prior

The methods presented in Section 2 allow to reconstruct the Dark Energy EoS as a function of redshift starting from its binned values; however the  $w_i$  in each bin can in principle assume any value, with no relation to the values of the other bins. This does not take into account that viable theoretical models do not generally allow for extreme oscillations of this function [47], and therefore such a reconstruction can lead to a  $w_{\text{DE}}(a)$  that cannot be linked to any physically viable theoretical model. As already anticipated, we overcome this problem including a theoretically informed prior which account for the fact that a given  $w_i$  will be correlated with the values assumed by the function in the adjacent bins. Following the approach of [34] we impose a correlation prior, which rescales the Likelihood function ( $\mathcal{L}$ ) as

$$-\ln \mathcal{L} = \chi^2 = \chi_{\text{data}}^2 + \chi_{\text{prior}}^2, \quad (3.1)$$

where we assumed a Gaussian distribution  $\mathcal{L} \propto \exp[-\chi^2/2]$ . We define this prior as

$$\chi_{\text{prior}}^2 = (\mathbf{w} - \bar{\mathbf{w}})^T \mathcal{C}^{-1} (\mathbf{w} - \bar{\mathbf{w}}), \quad (3.2)$$

where  $\mathbf{w} = \{w_1, \dots, w_N\}$  is the vector containing the binned values of  $w_{\text{DE}}(a)$ ,  $\mathcal{C}$  is a covariance matrix and  $\bar{\mathbf{w}}$  is a vector composed by the expected values of  $w_{\text{DE}}$  in each bin. To avoid any specific choice for  $\bar{\mathbf{w}}$ , which could affect the final results, we define this as the mean value of the EoS in the bin under consideration and in the adjacent ones, i.e.

$$\bar{w}_i = \begin{cases} (w_i + w_{i+1})/2 & i = 1 \\ (w_{i-1} + w_i + w_{i+1})/3 & i = 2, \dots, N-1 \\ (w_{i-1} + 2w_i)/3 & i = N \end{cases} \quad (3.3)$$

where in the case of the last bin, we account for the fact that  $w(a < a_N) = w(a_N)$ . Including this prior distribution, means that we are assuming that our  $w_i$  parameters are Gaussian distributed and their fluctuations around  $\bar{\mathbf{w}}$  are described by the covariance matrix  $\mathcal{C}$ . Since we want this matrix to encode the theoretical correlation of the values of  $w_{\text{DE}}(a)$  at different redshifts,  $\mathcal{C}$  needs to be obtained imposing conditions arising from the physical viability of theoretical models. We use therefore the results of [32], where such a correlation was obtained in different Dark Energy and Modified Gravity models, imposing a set of viability and stability conditions, e.g. requiring the avoidance of ghosts and gradient instabilities.

Following [32] we write the covariance matrix as

$$\mathcal{C}(a, a') = \sqrt{C(a)C(a')} \tilde{\mathcal{C}}(a, a') \quad (3.4)$$



with  $C(a)$  an autocorrelation function and  $\tilde{C}(a, a')$  a correlation matrix, functions only of the scale factor.

We focus our analysis the class of canonical single field Quintessence (from now on simply Quintessence), and on the broad class of Horndeski gravity. Despite somewhat limiting the model independence of our approach, we can still analyze a broad class of models, ensuring at the same time that the results we obtain will correspond to theoretical models which satisfy physical viability conditions.

We use  $C(a)$  and  $\tilde{C}(a, a')$  obtained by [32], where the numerical correlations found for different classes of DE and MG models were encoded in the fitting formulas shown in Table 1, where for  $\tilde{C}$  two possible choices are taken into account, i.e. an exponential and a CPZ parameterization. Both these choices are built in such a way that if  $\delta a = a_i - a_j$  (or  $\delta \ln(a) = \ln(a_i) - \ln(a_j)$ ) is much higher than the correlation length  $\xi$  then the correlation tends to zero. The prior that best minimizes the residuals in both the Quintessence and Horndeski cases is the exponential one [32].

Autocorrelation function		$\alpha$	$\beta$	$\gamma$	$x$
$C(x) = \alpha + \beta \exp[\gamma(x - x_0)]$	Quintessence	0.03	0.3	6.5	$a$
	Horndeski	0.05	0.8	2	$\ln(a)$
Correlation matrix		$\xi$	$n$	$x$	$y$
$\tilde{C}(x, y) = \exp \left[ \left( -\frac{ x-y }{\xi} \right)^n \right]$	Quintessence	0.7	1.8	$a$	$a'$
	Horndeski	0.3	1.2	$\ln(a)$	$\ln(a')$
$\tilde{C}(x, y) = \frac{1}{1 + \left( \frac{ x-y }{\xi} \right)^n}$	Quintessence	0.6	2	$a$	$a'$
	Horndeski	0.2	2	$\ln(a)$	$\ln(a')$

**Table 1.** Summary of the autocorrelation and correlation analytical fits obtained by [32]. The first parameterization of the correlation matrix is the exponential, while the second is the CPZ [34]. Here  $x_0$  denotes the  $x$  variable evaluated at present time, i.e.  $x_0 = a_0 = 1$  (or  $x_0 = \ln(a_0) = 0$ ).

We want to stress here that having a correlation length set by theoretical requirements significantly helps in the choice of the binning strategy, as the correlation length defines a number of effective degrees of freedom  $N_{\text{eff}} = (a_{\text{max}} - a_{\text{min}})/\xi$ ; as long as the number of bins  $N$  satisfies  $N > N_{\text{eff}}$ , the dependence of the reconstruction on the number of bins is negligible [34].

The specific analysis strategy will depend on the class of models under consideration. Quintessence models modify the background expansion of the Universe with respect to  $\Lambda$ CDM without modifying the equations for the evolution of cosmological perturbations; therefore we can use both background (SN and BAO) and perturbation (CMB) data. On the contrary, for Horndeski models the use of CMB data would require us to consider also their impact on the growth of cosmological structures, eventually jointly binning the phenomenological functions  $\mu$  and  $\Sigma$  [22, 48]. Since the reconstruction of these two functions is beyond the scope of this paper, we limit our analysis in this case to background data only.

The two classes of models also have different requirements for the prior range:

- **Quintessence:** the EoS lies in the region above the Phantom divide ( $w = -1$ ), hence we impose  $w_{\text{DE}}(a) \geq -1$ . To this purpose we sample the  $w_i$  parameters in the range  $[-3, 0]$  but we then cut the posterior for each reconstruction parameter to  $w_i \geq -1$ . The reconstruction of  $w_{\text{DE}}(a)$  for Quintessence is done using both the CPZ and exponential correlation priors (Table 1), to highlight how they differently affect the inferred  $w_i$



parameters. Given the theoretical correlation length for this case ( $\xi_{exp} = 0.6 \sim \xi_{CPZ} = 0.7$ ) the  $w_i$  parameters are defined in the bins  $\vec{a} = (0.85, 0.7, 0.55, 0.4, 0.25, 0.1)$  in order to satisfy the requirement  $N > N_{\text{eff}}$ .

- **Horndeski:** the EoS has no particular restriction in the values that it can assume, hence  $w_i$  is sampled in the range  $[-3, 0]$  and no cut is applied. The reconstruction for the Horndeski case is obtained using the exponential prior (Table 1). In this case the Planck CMB data are not included as we are not modelling the impact of this class of models on the evolution of perturbations. Also in this case, the choice of the scale factor range in which we define our bins is made in such a way to satisfy the requirement  $N > N_{\text{eff}}$ ; as the correlation length in this case is  $\xi_{exp} = 0.3$  we use  $\vec{a} = (0.9, 0.8, 0.7, 0.6, 0.5, 0.4)$ . In this case, since we are not using Planck data, the redshift range in which data are available is smaller than in the previous case, therefore we limit our reconstruction to  $a_6 = 0.4$  ( $z_6 = 1.5$ ).

We apply this prior information to our analysis both when using the smoothed step and GP reconstruction. It is worth stressing that in the latter case, the GP and prior both exploit a correlation between the values of  $w_{DE}(a)$  at different scale factors. However, while GP returns the value of  $w_{DE}$  at a given  $a_*$  given the  $w_i$ , without acting on the  $w_i$  itself, the correlation prior is related to the relative values of the different  $w_i$ , penalizing those configurations of binned values which do not satisfy the viability conditions. In this sense, the GP and correlation priors are complementary and their combined use is possible.

## 4 Results

In this Section we present the results obtained following the analysis method described in the previous two Sections, discussing separately the reconstruction within the Quintessence realm and that for the more general Horndeski class.

### 4.1 Quintessence

We report the results for Quintessence in Table 2. The results are obtained both with and without the inclusion of the theoretical prior (exponential and CPZ), for comparison. In all three cases, we find only upper limits on the  $w_i$  parameters, with the lower bound  $w = -1$  included within the  $1-\sigma$  bound, thus indicating that these results are compatible with  $\Lambda$ CDM.

Figure 2 shows the results obtained reconstructing the DE EoS via the smoothed step function. We point out that the mean values of the reconstruction deviate from the  $\Lambda$ CDM limit given the requirement of a hard bound for the posterior at  $w_i = -1$ , which however does not prevent  $\Lambda$ CDM from being a good fit for this reconstruction.

The comparison of the three cases, bin by bin, can be quantified as a percentage difference of the mean values inferred adding the exponential (exp) and CPZ priors with respect to the mean values obtained with no theoretical prior. The main differences associated to the choice of a particular prior are related to the behavior of  $w_4$  (exp:  $-1.32\%$ , CPZ:  $-0.44\%$ ),  $w_5$  (exp:  $-3.3\%$ , CPZ:  $-2.01\%$ ) and  $w_6$  (exp:  $-4.3\%$ , CPZ:  $-2.47\%$ ) mean values and  $1\sigma$  confidence levels, while  $w_1$  (exp:  $-0.249\%$ , CPZ:  $0\%$ ),  $w_2$  (exp:  $+0.214\%$ , CPZ:  $+0.107\%$ ) and  $w_3$  (exp:  $0\%$ , CPZ:  $+0.108\%$ ) do not differ significantly case by case. The larger impact of the correlation priors in the last three bins can be explained with the fact that these redshifts contain much less data; therefore the constraining power of the prior is comparable to that of the data.

SMOOTHED STEP FUNCTION RECONSTRUCTION			
Parameter	Planck+BAO+SN	Planck+BAO+SN (exp prior)	Planck+BAO+SN (CPZ prior)
$\Omega_b h^2$ .....	$0.02242 \pm 0.00021$	$0.02242 \pm 0.00021$	$0.02242 \pm 0.00021$
$\Omega_c h^2$ .....	$0.1164 \pm 0.0015$	$0.1165 \pm 0.0015$	$0.1166 \pm 0.0015$
$H_0$ .....	$65.1^{+1.6}_{-0.94}$	$65.1^{+1.6}_{-0.95}$	$65.1^{+1.5}_{-0.94}$
$\Omega_\Lambda$ .....	$0.670^{+0.017}_{-0.0099}$	$0.670^{+0.016}_{-0.010}$	$0.670^{+0.016}_{-0.0099}$
$\Omega_m$ .....	$0.330^{+0.0099}_{-0.017}$	$0.330^{+0.010}_{-0.016}$	$0.3296^{+0.0099}_{-0.016}$
$w_1$ .....	$< -0.757$	$< -0.759$	$< -0.761$
$w_2$ .....	$< -0.926$	$< -0.924$	$< -0.923$
$w_3$ .....	$< -0.916$	$< -0.914$	$< -0.914$
$w_4$ .....	$< -0.891$	$< -0.895$	$< -0.902$
$w_5$ .....	$< -0.820$	$< -0.831$	$< -0.844$
$w_6$ .....	$< -0.708$	$< -0.732$	$< -0.750$

**Table 2.** Mean values and  $1\sigma$  confidence levels or upper limits of the Quintessence case inferred parameters, using the datasets without and with the priors, reconstructing the Equation of State via smoothed step function. The input scale factors associated to the  $\vec{w}$  are  $\vec{a} = (0.85, 0.7, 0.55, 0.4, 0.25, 0.1)$ .

The prior however, does not impact significantly the behavior of the function, showing how the requirement  $w_i \geq -1$  already satisfies the physical viability conditions imposed through the correlation prior.

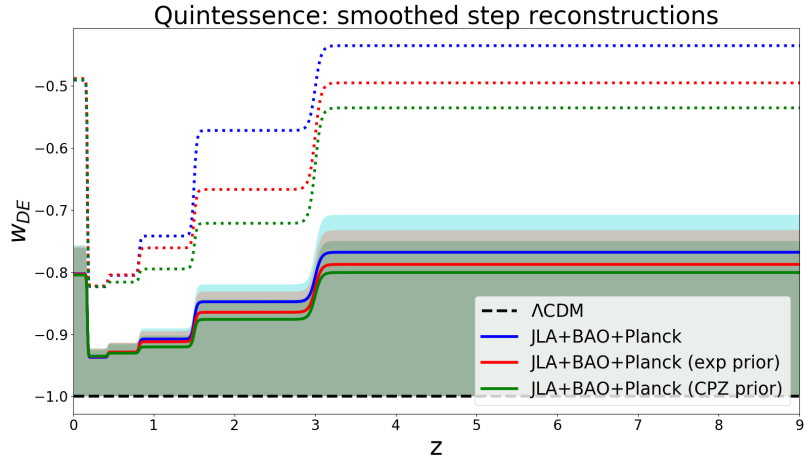


**Figure 2.** Reconstructed mean values of  $w_{DE}(a)$  in the Quintessence case, obtained via smoothed step function. The blue line corresponds to the reconstruction without the inclusion of any theoretical prior on the correlation of  $w_i$  parameters, while the red and green line are obtained including the exponential and CPZ correlations respectively. The filled areas of the corresponding colors trace the  $1\sigma$  confidence levels, while the dotted lines delimit the  $2\sigma$  confidence levels. The input scale factors are  $\vec{a} = (0.85, 0.7, 0.55, 0.4, 0.25, 0.1)$ .

In order to test the dependence of the results on the reconstruction method, we perform the analysis for the Quintessence class, both with Planck+BAO+SN only and with the

inclusion of the CPZ prior, using the Gaussian Process reconstruction method rather than the smoothed bins one. In this case, we fix the correlation length  $\xi$  of the GP to that of the theoretical prior. Furthermore, we choose to force  $w_{\text{DE}}(a)$  to remain constant at the value of the first redshift bin  $w_1$  for  $a > a_1$ .

GAUSSIAN PROCESS RECONSTRUCTION		
Parameter	Planck+BAO+SN	Planck+BAO+SN (CPZ prior)
$\Omega_b h^2$ .....	$0.02242^{+0.00022}_{-0.00020}$	$0.02241 \pm 0.00021$
$\Omega_c h^2$ .....	$0.1166 \pm 0.0015$	$0.1167 \pm 0.0014$
$H_0$ .....	$62.8^{+1.6}_{-2.0}$	$63.4^{+2.2}_{-1.6}$
$\Omega_\Lambda$ .....	$0.645 \pm 0.020$	$0.651^{+0.025}_{-0.017}$
$\Omega_m$ .....	$0.355 \pm 0.020$	$0.349^{+0.017}_{-0.025}$
$w_1$ .....	$< -0.764$	$< -0.723$
$w_2$ .....	$< -0.916$	$< -0.933$
$w_3$ .....	$< -0.914$	$< -0.901$
$w_4$ .....	$< -0.889$	$< -0.911$
$w_5$ .....	$< -0.816$	$< -0.833$
$w_6$ .....	$< -0.691$	$< -0.726$

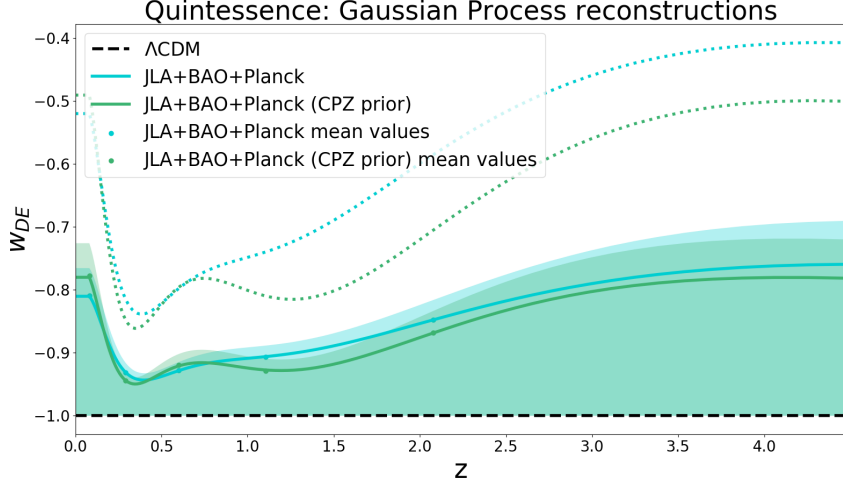
**Table 3.** Mean values and  $1\sigma$  confidence levels of the Quintessence case inferred parameters, using the datasets without and with the CPZ prior, reconstructing the Equation of State via Gaussian Process method. The input scale factors associated to the  $\vec{w}$  are  $\vec{a} = (0.85, 0.7, 0.55, 0.4, 0.25, 0.1)$ .

Table 3 shows the results obtained on the cosmological and reconstruction parameters in the Planck+BAO+SN and Planck+BAO+SN+prior cases, while in Figure 3 we show the reconstruction of the  $w_{\text{DE}}(a)$  function given the mean values of  $w_i$ . We notice how the results are compatible with the smoothed bins reconstruction, but with the prior affecting more significantly than before the earliest redshifts of the reconstruction: the mean values of the reconstruction obtained adding the prior respectively differ from the  $w_1$ ,  $w_2$  and  $w_3$  means obtained with only the datasets by +4.2%, -1.5% and +0.86%. These results are emphasized by the comparison shown in Figure 4.

## 4.2 Horndeski class of MG models

In Table 4 we report the results obtained reconstructing the EoS via smoothed step function and GP in the Horndeski case, for which the  $w_i$  parameters are free to vary within the range  $[-3, 0]$  and the exponential correlation prior is imposed. As already mentioned, in this case we restrict to background data, and do not use CMB measurements. In both cases the last bin considered  $w_6$  is unconstrained due to the fact that very few data are available at this redshift ( $z \sim [1, 1.5]$ ). Because of the correlation that we have introduced between the binned values of  $w_{\text{DE}}$ , this lack of constraining power propagates also to the constraints at higher scale factors (lower redshifts). For the other bins, we obtain compatible constraints from the two reconstruction methods, in agreement within  $1\sigma$  with each other and with a  $\Lambda$ CDM expansion history. Notice that in this case, with  $w_{\text{DE}}(a)$  able to take values below -1 and with no CMB data, we do not have constraining power on  $H_0$ .

In Figure 5 we show the reconstruction of  $w_{\text{DE}}(a)$  given the inferred  $w_i$  using both the smoothed and Gaussian process reconstruction methods. The function tends to decrease over redshift, independently of the reconstruction method, with the mean reconstructed function



**Figure 3.** Reconstructed mean values of  $w_{\text{DE}}(a)$  in the Quintessence case, obtained via Gaussian Process. The cyan line corresponds to the reconstruction without the inclusion of any theoretical prior on the correlation of  $w_i$  parameters, while the green line is obtained including the CPZ correlation. The filled areas of the corresponding colors trace the  $1\sigma$  confidence levels, while the dotted lines delimit the  $2\sigma$  confidence levels. The input scale factors are  $\vec{a} = (0.85, 0.7, 0.55, 0.4, 0.25, 0.1)$ .

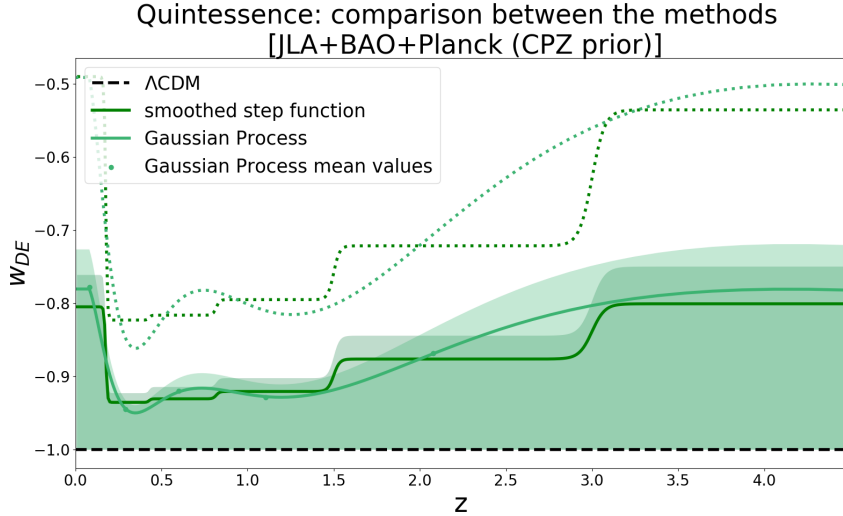


**Figure 4.** Superposition of the smoothed step function and Gaussian Process reconstructions for Quintessence Equation of State obtained including the datasets and the CPZ prior. For each case, the continuous lines are the reconstructions obtained using the mean values, whereas the filled areas of the corresponding colours trace the  $1\sigma$  confidence levels, while the dotted lines delimit the  $2\sigma$  confidence levels. The input scale factors are  $\vec{a} = (0.85, 0.7, 0.55, 0.4, 0.25, 0.1)$ .

closer to the  $\Lambda\text{CDM}$  value in the GP case; however, results from the two methods are still compatible within  $1\sigma$ .

The inclusion of CMB data also in the Horndeski case would increase the amount of

RECONSTRUCTIONS: JLA+BAO (exp prior)		
Parameter	Smoothed step function	Gaussian Process
$\Omega_b h^2$ .....	$0.041^{+0.012}_{-0.031}$	$0.049^{+0.017}_{-0.031}$
$\Omega_c h^2$ .....	$0.181^{+0.084}_{-0.12}$	$0.157^{+0.067}_{-0.10}$
$H_0$ .....	$> 76.6$	$> 79.7$
$\Omega_\Lambda$ .....	$0.684 \pm 0.086$	$0.713 \pm 0.072$
$\Omega_m$ .....	$0.316 \pm 0.086$	$0.287 \pm 0.072$
$w_1$ .....	$-1.10^{+0.30}_{-0.22}$	$-1.10^{+0.28}_{-0.23}$
$w_2$ .....	$-0.97^{+0.36}_{-0.22}$	$-0.86^{+0.26}_{-0.18}$
$w_3$ .....	$-1.09^{+0.60}_{-0.30}$	$-0.98^{+0.44}_{-0.25}$
$w_4$ .....	$-1.21^{+0.73}_{-0.39}$	$-1.05^{+0.58}_{-0.34}$
$w_5$ .....	$-1.44^{+0.75}_{-0.63}$	$-1.36^{+0.74}_{-0.62}$
$w_6$ .....	unconstrained	unconstrained

**Table 4.** Mean values and  $1\sigma$  confidence levels of the Horndeski case, reconstructing the Equation of State via smoothed step function and via Gaussian Process. The input scale factors associated to the  $\vec{w}$  are  $\vec{a} = (0.9, 0.8, 0.7, 0.6, 0.5, 0.4)$ . Here  $w_6$  is unconstrained, with the  $1\sigma$  region extending over the full prior range.

information and potentially improve the constraints achievable with this method; however, as already pointed out, this would require the reconstruction of the  $\mu(a)$  and  $\Sigma(a)$  encoding the departures from the standard  $\Lambda$ CDM growth of cosmological perturbations. The possible degeneracies between the effects of these two functions and those of a varying  $w_{\text{DE}}(a)$  can therefore limit the improvement in the achievable constraints when CMB data are included. A full analysis of this scenario would therefore require the use of cosmological data able to disentangle the background and perturbation modifications, e.g. Cosmic Shear or Galaxy Clustering data from Large Scale Structure surveys [8, 49, 50].

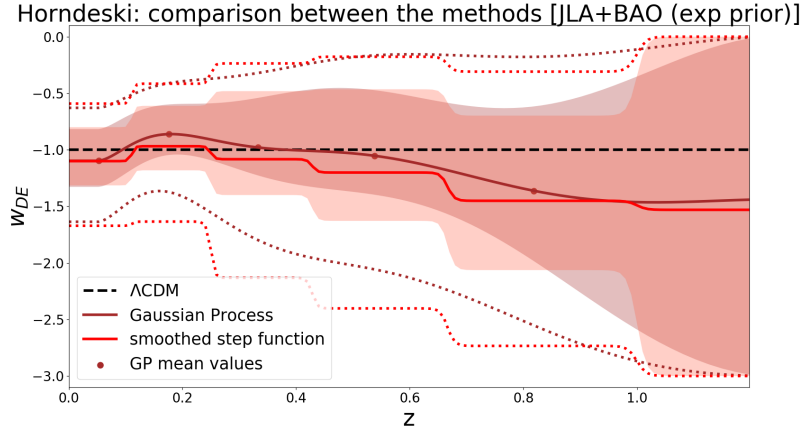


**Figure 5.** Superposition of the smoothed step function and Gaussian Process reconstructions for the Equation of State in the Horndeski case, obtained including the datasets and the exponential prior. For each case, the continuous lines are the reconstructions obtained using the mean values, whereas the filled areas of the corresponding colours trace the  $1\sigma$  confidence levels, while the dotted lines delimit the  $2\sigma$  confidence levels. The input scale factors are  $\vec{a} = (0.9, 0.8, 0.7, 0.6, 0.5, 0.4)$ .

## 5 Conclusions

We have reconstructed the Equation of State (EoS) of Dark Energy,  $w_{\text{DE}}(a)$ , from the latest cosmological data with two different techniques: one in which the EoS is assumed constant within the range of each specified bin in scale factor, with smooth transitions between binned values; and one in which the function is reconstructed at each value of  $a$  from its binned values using a Gaussian Process reconstruction. We modified the public code **CAMB** to produce predictions on cosmological observables given the reconstructed  $w_{\text{DE}}(a)$  and we compared these predictions with currently available data both for background (SN and BAO) and for perturbations (CMB) observables. Alongside the observational data, we took into account the contribution of theoretical conditions on the physical viability of the reconstructed EoS; this was possible with the inclusion of a correlation prior between the binned values of  $w_{\text{DE}}(a)$ , obtained in two classes of models: single field Quintessence and Horndeski gravity [32].

The analysis of these two classes differs both in the binning strategy for  $w_{\text{DE}}(a)$ , which is defined by the different correlation lengths  $\xi$ , and in the observables used to constrain the parameters: in the Quintessence case, the reconstruction of  $w_{\text{DE}}(a)$  was sufficient to fully characterize the modification on background and perturbations evolutions with respect to  $\Lambda\text{CDM}$  and we can therefore use all the data from BAO, SN and CMB. In the Horndeski case instead, the description of perturbations would have required also to reconstruct the  $\mu(a)$  and  $\Sigma(a)$ , and therefore we limited our analysis to the background data coming from BAO and SN observations. Moreover, while for Horndeski the binned values  $w_i$  were allowed to vary in the full prior range  $[-3, 0]$ , this range was limited in Quintessence to  $[-1, 0]$  as these models cannot cross the phantom divide  $w = -1$  without developing ghost instabilities.

In our results for the Quintessence case, we found that  $\Lambda\text{CDM}$   $w = -1$  is compatible with the reconstructed  $w_{\text{DE}}(a)$  within  $1\sigma$ . Moreover we found that the theoretical prior is not affecting the results significantly, due to the limitation of our analysis to the non-phantom part of the parameter space ( $w_i \geq -1$ ) which already satisfies the most restrictive

of the physical viability conditions [33]. The results of the two reconstruction methods are in agreement with each other, highlighting how for a high enough number of bins, the smoothed bins reconstruction is able to reproduce sufficient variations of  $w$  in redshift to fit cosmological data.

In the Horndeski case, we also found that  $w = -1$  is compatible with the reconstructed EoS within  $1\sigma$ . The smoothed bins and GP reconstruction methods are found to be compatible also in this case, although less than in the Quintessence analysis; this is possibly due to the fact that the oscillatory behavior hinted by the reconstruction could require a higher number of bins to be reproduced in the smoothed bins case, or that a different GP Kernel would be more appropriate for such behavior. Tighter constraints on the EoS, that would allow to quantify the impact of the theoretical prior also for this class of models, could be obtained including CMB data in the analysis, which requires to simultaneously reconstruct the phenomenological functions describing deviations from  $\Lambda$ CDM in clustering and lensing, respectively  $\mu$  and  $\Sigma$ . As we discussed, given the degeneracies between the effects of  $w$ ,  $\mu$  and  $\Sigma$ , additional observables would be needed for this kind of analysis, e.g. coming from observations of Large Scale Structures.

## Acknowledgments

We want to thank Simone Peirone, Marco Raveri and Robert Crittenden for useful discussions. MM acknowledges support from the D-ITP consortium, a program of the NWO that is funded by the OCW. AS acknowledges support from the NWO and the Dutch Ministry of Education, Culture and Science (OCW), and from the D-ITP consortium, a program of the NWO that is funded by the OCW.

## References

- [1] Adam G. Riess et al. Observational evidence from supernovae for an accelerating universe and a cosmological constant. *Astron. J.*, 116:1009–1038, 1998.
- [2] S. Perlmutter et al. Measurements of Omega and Lambda from 42 high redshift supernovae. *Astrophys. J.*, 517:565–586, 1999.
- [3] N. Aghanim et al. Planck 2018 results. VI. Cosmological parameters. 2018.
- [4] Steven Weinberg. The Cosmological Constant Problem. *Rev. Mod. Phys.*, 61:1–23, 1989. [569(1988)].
- [5] C. P. Burgess. The Cosmological Constant Problem: Why it’s hard to get Dark Energy from Micro-physics. In *Proceedings, 100th Les Houches Summer School: Post-Planck Cosmology: Les Houches, France, July 8 - August 2, 2013*, pages 149–197, 2015.
- [6] A. G. Riess, S. Casertano, W. Yuan, L. Macri, J. Anderson, J. W. MacKenty, J. B. Bowers, K. I. Clubb, A. V. Filippenko, D. O. Jones, and B. E. Tucker. New Parallaxes of Galactic Cepheids from Spatially Scanning the Hubble Space Telescope: Implications for the Hubble Constant. *The Astrophysical Journal*, 855:136, March 2018.
- [7] Catherine Heymans et al. CFHTLenS tomographic weak lensing cosmological parameter constraints: Mitigating the impact of intrinsic galaxy alignments. *Mon. Not. Roy. Astron. Soc.*, 432:2433, 2013.
- [8] F. Köhlinger et al. KiDS-450: The tomographic weak lensing power spectrum and constraints on cosmological parameters. *Mon. Not. Roy. Astron. Soc.*, 471(4):4412–4435, 2017.



- [9] T. M. C. Abbott et al. Dark Energy Survey year 1 results: Cosmological constraints from galaxy clustering and weak lensing. *Phys. Rev.*, D98(4):043526, 2018.
- [10] Tamara M. Davis et al. Scrutinizing Exotic Cosmological Models Using ESSENCE Supernova Data Combined with Other Cosmological Probes. *Astrophys. J.*, 666:716–725, 2007.
- [11] Luca Amendola, Martin Kunz, and Domenico Sapon. Measuring the dark side (with weak lensing). *JCAP*, 0804:013, 2008.
- [12] Takeshi Chiba, Antonio De Felice, and Shinji Tsujikawa. Observational constraints on quintessence: thawing, tracker, and scaling models. *Phys. Rev.*, D87(8):083505, 2013.
- [13] Matteo Cataneo, David Rapetti, Fabian Schmidt, Adam B. Mantz, Steven W. Allen, Douglas E. Applegate, Patrick L. Kelly, Anja von der Linden, and R. Glenn Morris. New constraints on  $f(R)$  gravity from clusters of galaxies. *Phys. Rev.*, D92(4):044009, 2015.
- [14] Alexander Bonilla and Jairo E. Castillo. Constraints On Dark Energy Models From Galaxy Clusters and Gravitational Lensing Data. *Universe*, 4(1):21, 2018.
- [15] Sixiang Wen, Shuang Wang, and Xiaolin Luo. Comparing dark energy models with current observational data. *JCAP*, 1807(07):011, 2018.
- [16] Malcolm Fairbairn and Ariel Goobar. Supernova limits on brane world cosmology. *Phys. Lett.*, B642:432–435, 2006.
- [17] Roy Maartens and Elisabetta Majerotto. Observational constraints on self-accelerating cosmology. *Phys. Rev.*, D74:023004, 2006.
- [18] Sara Rydbeck, Malcolm Fairbairn, and Ariel Goobar. Testing the DGP model with ESSENCE. *JCAP*, 0705:003, 2007.
- [19] Yong-Seon Song, Ignacy Sawicki, and Wayne Hu. Large-Scale Tests of the DGP Model. *Phys. Rev.*, D75:064003, 2007.
- [20] Michel Chevallier and David Polarski. Accelerating universes with scaling dark matter. *Int. J. Mod. Phys.*, D10:213–224, 2001.
- [21] Eric V. Linder. Exploring the expansion history of the universe. *Phys. Rev. Lett.*, 90:091301, 2003.
- [22] P. A. R. Ade et al. Planck 2015 results. XIV. Dark energy and modified gravity. *Astron. Astrophys.*, 594:A14, 2016.
- [23] N. Suzuki, D. Rubin, C. Lidman, G. Aldering, R. Amanullah, K. Barbary, L. F. Barrientos, J. Botyanszki, M. Brodwin, N. Connolly, K. S. Dawson, A. Dey, M. Doi, M. Donahue, S. Deustua, P. Eisenhardt, E. Ellingson, L. Faccioli, V. Fadeyev, H. K. Fakhouri, A. S. Fruchter, D. G. Gilbank, M. D. Gladders, G. Goldhaber, A. H. Gonzalez, A. Goobar, A. Gude, T. Hattori, H. Hoekstra, E. Hsiao, X. Huang, Y. Ihara, M. J. Jee, D. Johnston, N. Kashikawa, B. Koester, K. Konishi, M. Kowalski, E. V. Linder, L. Lubin, J. Melbourne, J. Meyers, T. Morokuma, F. Munshi, C. Mullis, T. Oda, N. Panagia, S. Perlmutter, M. Postman, T. Pritchard, J. Rhodes, P. Ripoche, P. Rosati, D. J. Schlegel, A. Spadafora, S. A. Stanford, V. Stanishev, D. Stern, M. Strovink, N. Takanashi, K. Tokita, M. Wagner, L. Wang, N. Yasuda, H. K. C. Yee, and The Supernova Cosmology Project. The Hubble Space Telescope Cluster Supernova Survey. V. Improving the Dark-energy Constraints above  $z \gtrsim 1$  and Building an Early-type-hosted Supernova Sample. *ApJ*, 746:85, February 2012.
- [24] Robert J. Scherrer. Mapping the Chevallier-Polarski-Linder parametrization onto Physical Dark Energy Models. *Phys. Rev.*, D92(4):043001, 2015.
- [25] R. Laureijs, J. Amiaux, S. Arduini, J. . Auguères, J. Brinchmann, R. Cole, M. Cropper, C. Dabin, L. Duvet, A. Ealet, and et al. Euclid Definition Study Report. *ArXiv e-prints*, October 2011.

- [26] T. Holsclaw, U. Alam, B. Sansó, H. Lee, K. Heitmann, S. Habib, and D. Higdon. Nonparametric Dark Energy Reconstruction from Supernova Data. *Physical Review Letters*, 105(24):241302, December 2010.
- [27] T. Holsclaw, U. Alam, B. Sansó, H. Lee, K. Heitmann, S. Habib, and D. Higdon. Nonparametric reconstruction of the dark energy equation of state. *Phys. Rev. D*, 82(10):103502, November 2010.
- [28] M. Seikel, C. Clarkson, and M. Smith. Reconstruction of dark energy and expansion dynamics using Gaussian processes. *J. Cosmology Astropart. Phys.*, 6:036, June 2012.
- [29] Y. Wang, L. Pogosian, G.-B. Zhao, and A. Zucca. Evolution of dark energy reconstructed from the latest observations. *ArXiv e-prints*, July 2018.
- [30] Najla Said, Carlo Baccigalupi, Matteo Martinelli, Alessandro Melchiorri, and Alessandra Silvestri. New Constraints On The Dark Energy Equation of State. *Phys. Rev.*, D88:043515, 2013.
- [31] Arman Shafieloo, Ujjaini Alam, Varun Sahni, and Alexei A. Starobinsky. Smoothing Supernova Data to Reconstruct the Expansion History of the Universe and its Age. *Mon. Not. Roy. Astron. Soc.*, 366:1081–1095, 2006.
- [32] Marco Raveri, Philip Bull, Alessandra Silvestri, and Levon Pogosian. Priors on the effective dark energy equation of state in scalar-tensor theories. *Phys. Rev. D*, 96:083509, Oct 2017.
- [33] Simone Peirone, Matteo Martinelli, Marco Raveri, and Alessandra Silvestri. Impact of theoretical priors in cosmological analyses: the case of single field quintessence. *Phys. Rev.*, D96(6):063524, 2017.
- [34] Robert G. Crittenden, Levon Pogosian, and Gong-Bo Zhao. Investigating dark energy experiments with principal components. *Journal of Cosmology and Astroparticle Physics*, 2009(12):025, 2009.
- [35] S. Casas, M. Kunz, M. Martinelli, and V. Pettorino. Linear and non-linear Modified Gravity forecasts with future surveys. *Physics of the Dark Universe*, 18:73–104, December 2017.
- [36] Carl Edward Rasmussen and Chris Williams. *Gaussian Processes for Machine Learning*. 2006.
- [37] Balakrishna S. Haridasu, Vladimir V. Lukovič, Michele Moresco, and Nicola Vittorio. An improved model-independent assessment of the late-time cosmic expansion. *JCAP*, 1810(10):015, 2018.
- [38] Antony Lewis, Anthony Challinor, and Anthony Lasenby. Efficient computation of CMB anisotropies in closed FRW models. *Astrophys. J.*, 538:473–476, 2000.
- [39] Cullan Howlett, Antony Lewis, Alex Hall, and Anthony Challinor. CMB power spectrum parameter degeneracies in the era of precision cosmology. *J. Cosmology Astropart. Phys.*, 1204:027, 2012.
- [40] Antony Lewis and Sarah Bridle. Cosmological parameters from CMB and other data: A Monte Carlo approach. *Phys. Rev.*, D66:103511, 2002.
- [41] M. Betoule et al. Improved cosmological constraints from a joint analysis of the SDSS-II and SNLS supernova samples. *Astron. Astrophys.*, 568:A22, 2014.
- [42] Masao Sako et al. The Data Release of the Sloan Digital Sky Survey-II Supernova Survey. *Publ. Astron. Soc. Pac.*, 130:064002, 2018.
- [43] J. Guy, M. Sullivan, A. Conley, N. Regnault, P. Astier, C. Balland, S. Basa, R. G. Carlberg, D. Fouchez, D. Hardin, I. M. Hook, D. A. Howell, R. Pain, N. Palanque-Delabrouille, K. M. Perrett, C. J. Pritchett, J. Rich, V. Ruhlmann-Kleider, D. Balam, S. Baumont, R. S. Ellis, S. Fabbro, H. K. Fakhouri, N. Fourmanoit, S. González-Gaitán, M. L. Graham, E. Hsiao, T. Kronborg, C. Lidman, A. M. Mourao, S. Perlmutter, P. Ripoche, N. Suzuki, and E. S.

Walker. The Supernova Legacy Survey 3-year sample: Type Ia supernovae photometric distances and cosmological constraints. *Astron. Astrophys.*, 523:A7, November 2010.

- [44] Florian Beutler, Chris Blake, Matthew Colless, D. Heath Jones, Lister Staveley-Smith, Lachlan Campbell, Quentin Parker, Will Saunders, and Fred Watson. The 6df galaxy survey: baryon acoustic oscillations and the local hubble constant. *Monthly Notices of the Royal Astronomical Society*, 416(4):3017–3032, 2011.
- [45] Ashley J. Ross, Lado Samushia, Cullan Howlett, Will J. Percival, Angela Burden, and Marc Manera. The clustering of the sdss dr7 main galaxy sample – a 4 per cent distance measure at  $z = 0.15$ . *Monthly Notices of the Royal Astronomical Society*, 449(1):835–847, 2015.
- [46] Planck Collaboration, P. A. R. Ade, et al. Planck 2015 results. XIII. Cosmological parameters. *Astron. Astrophys.*, 594:A13, September 2016.
- [47] Robert G. Crittenden, Gong-Bo Zhao, Levon Pogosian, Lado Samushia, and Xinmin Zhang. Fables of reconstruction: controlling bias in the dark energy equation of state. *Journal of Cosmology and Astroparticle Physics*, 2012(02):048, 2012.
- [48] Levon Pogosian and Alessandra Silvestri. What can cosmology tell us about gravity? constraining horndeski gravity with  $\Sigma$  and  $\mu$ . *Phys. Rev. D*, 94:104014, Nov 2016.
- [49] T. M. C. Abbott et al. Dark Energy Survey year 1 results: Cosmological constraints from galaxy clustering and weak lensing. *Phys. Rev.*, D98(4):043526, 2018.
- [50] H. Hildebrandt et al. KiDS-450: Cosmological parameter constraints from tomographic weak gravitational lensing. *Mon. Not. Roy. Astron. Soc.*, 465:1454, 2017.